Journal of Quantitative Spectroscopy & Radiative Transfer 112 (2011) 1581–1594

Contents lists available at ScienceDirect

Journal of Quantitative Spectroscopy & Radiative Transfer

journal homepage: www.elsevier.com/locate/jqsrt

Light absorption and scattering by aggregates: Application to black carbon and snow grains

K.N. Liou [a], Y. Takano [a,*], P. Yang [b]

[a] Joint Institute for Regional Earth System Science and Engineering, and Department of Atmospheric and Oceanic Sciences, University of California, Los Angeles, CA 90095, USA

[b] Department of Atmospheric Sciences, Texas A&M University, College Station, TX 77845, USA

ARTICLE INFO

Article history:
Received 16 January 2011
Received in revised form
22 February 2011
Accepted 9 March 2011
Available online 16 March 2011

Keywords:
Geometric optics
Monte Carlo photon tracing
Surface waves
Black carbon
Snow grain
Aggregate aerosol

ABSTRACT

A geometric-optics surface-wave approach has been developed for the computation of light absorption and scattering by nonspherical particles for application to aggregates and snow grains with external and internal mixing structures. Aggregates with closed- (internal mixing) and open-cell configurations are constructed by means of stochastic procedures using homogeneous and core-shell spheres with smooth or rough surfaces as building blocks. The complex aggregate shape and composition can be accounted for by using the hit-and-miss Monte Carlo geometric photon tracing method. We develop an integral expression for diffraction by randomly oriented aggregates based on Babinet's principle and a photon-number weighted geometric cross section. With reference to surface-wave contributions originally developed for spheres, we introduce a nonspherical correction factor using a non-dimensional volume parameter such that it is 1 for spheres and 0 for elongated particles. The extinction efficiency, single-scattering albedo, and asymmetry factor results for randomly oriented columns and plates compare reasonably well with those determined from the finite-difference time domain (FDTD) and the discrete dipole approximation (DDA) computer codes for size parameters up to about 20. The present theoretical approach covers all size ranges and is particularly attractive from the perspective of efficient light absorption and scattering calculations for complex particle shape and inhomogeneous composition.

We show that under the condition of equal volume and mass, the closed-cell configuration has larger absorption than its open-cell counterpart for both ballistic and diffusion-limited aggregates. Because of stronger absorption in the closed-cell case, most of the scattered energy is confined to forward directions, leading to a larger asymmetry factor than the open-cell case. Additionally, light absorption for randomly oriented snowflakes is similar to that of their spherical counterparts under the condition of equal geometrical cross section area for both external and internal mixing states; however, nonspherical snowflakes scatter less light in forward directions than spheres, resulting in a substantial reduction of the asymmetry factor. We further demonstrate that small soot particles on the order of 1 μm internally mixed with snow grains could effectively reduce snow albedo by as much as 5–10%. Indeed, the depositions of black carbon would substantially reduce mountain-snow albedo, which would lead to surface warming and snowmelt, critical to regional climatic surface temperature amplification and feedback.

* Corresponding author. Tel.: +1 310 794 9832; fax: +1 310 794 9796.
E-mail address: ytakano@atmos.ucla.edu (Y. Takano).

0022-4073/$ - see front matter © 2011 Elsevier Ltd. All rights reserved.
doi:10.1016/j.jqsrt.2011.03.007

1. Introduction

Understanding the direct and indirect radiative forcings of aerosols requires both fundamental knowledge and reliable data concerning their scattering and absorption properties. The single-scattering properties of aerosols are determined by their size, shape, and refractive index associated with chemical composition. Aerosol geometrical shapes are diverse, ranging from quasi-spherical to highly irregular. In addition to complex particle geometry, the inhomogeneous composition of aerosols has been commonly observed. Black carbon (BC) particles, which have highly complex and often inhomogeneous morphologies, are a type of aerosols that profoundly affects global and regional climates.

In the atmosphere, BCs strongly absorb sunlight, heat the air, and contribute to global warming [1,2]. Recent investigations indicate that the magnitude of the direct radiative forcing due to BC exceeds that from methane and may be the second most important component of global warming after carbon dioxide in terms of direct forcing [3,4]. In addition to the direct climate effect, BC particles, acting as CCN, can inhibit cloud formation [5]. The magnitude of BC absorption greatly depends on its refractive index (especially its imaginary part), shape, and size distribution; it also depends on the mixing state of BC particles. BCs are byproducts of solid, liquid, or vapor combustions, generated directly through the aggregation of molecules formed in combustion processes from coal, biomass burning, and biofuel. Recent estimates place the global emission of BC aerosols from biomass burning at 6–9 Tg/yr, and from fossil fuel burning at 6–8 Tg/yr [6]. BC emission levels have been especially high in China, due to the low-temperature household burning of coal and biofuels [7]. Model simulation results have suggested that anthropogenic fossil fuel soot exerts a positive radiative forcing of 0.5–2 W/m^2 at the top of the atmosphere [8] and that BCs produced in China induce a positive radiative forcing at the top of the atmosphere and a negative forcing at the surface [9]. However, reducing uncertainties in direct radiative forcing due to BC depends on an accurate accounting of its fundamental absorption and scattering properties.

BC particles can be internally and externally mixed with other nonabsorbing materials [10]. The identical amount of BC under different types of mixing can result in fairly different absorption properties. The efficiency of absorption of a certain amount of BC is determined by its mass absorption coefficient, which depends on particle size and the type of mixing between BC and nonabsorbing components, such as organic matter and sulfates. In the case of an external mixture where individual pure BC particles are parallel to nonabsorbing particles, the BC mass absorption efficiency is about the same for pure BC particles. However, BC particles that form at relatively high temperatures are likely to be coated by a nonabsorbing shell to form an internal mixture. Another type of internal mixture is a long-chain aggregate of BC particles formed at high temperatures, which can also be coated with nonabsorbing materials to form an internally mixed heterogeneous structure. These opened clusters usually collapse to form closely packed sphere-like structures as a result of aging or interactions with water vapor and clouds. Owing to their production mechanisms, BCs are confined to the 0.01 μm size range. However, aggregation of freshly produced particles may yield particle sizes above that range. Small spherical soot particles coagulate to form chain-like aggregates. These irregularly shaped particles have been found to be fractal, and have special optical properties. The mass median diameter of BC in the atmosphere is small, between 0.1 and 0.5 μm. In urban air, two size modes can often be detected: a smaller mode resulting from freshly formed primary aerosols and a larger mode resulting from coagulation processes. Because of their small size, BC aerosols normally have a long lifespan in the atmosphere.

The radiative transfer schemes that have been used in GCMs and climate models have not taken into account the effects of aerosol nonsphericity and inhomogeneous structure. Neglecting these effects could substantially underestimate or overestimate aerosol radiative forcing [11]. For example, the asymmetry factor of realistic aerosols, which is directly related to the albedo effect, can differ significantly from their spherical counterparts [12]. It follows that a spherical "equivalence" (and homogeneous) assumption can lead to erroneous assessment of aerosol radiative forcing. "Exact" numerical and theoretical solutions for scattering and absorption for realistic irregular ice particles and aerosols in planetary atmospheres that are consistent with the first principle appear to be extremely difficult, if not impossible, in view of the complexity and intricacy of their shape, size, and composition. In the following, we briefly review the methodologies that have been developed for the studies of light absorption and scattering by aggregates.

A number of computer models have been developed to simulate diffusion-limited aggregates and fractal clusters for light absorption studies [13–15]. Several authors have undertaken various approaches, including the Volume Integral Equation Formulation, the method of moments, the Extended Boundary Condition Method, and other approaches to calculate the scattering and absorption of aerosol particles with branched-chain structures and cluster of spheres [16–20]. Microwave analog experiments have been used to determine the light-scattering properties of aggregates for a combination of composition, size, and shape [21]. The optical properties of particulate carbon in terms of the material composition and morphology of soot have been evaluated to investigate their effects on extinction efficiency of aggregates and internal mixing of carbon with sulfate [22]. Light scattering by aggregates has also been computed from the T-matrix method to investigate the optical properties of comet dust [23]. Moreover, the scattering properties of randomly oriented soot aggregates consisting of fractal clusters of small homogeneous spherules have been extensively studied using the superposition T-matrix method [24–26].

We have developed a geometric optics approach coupled with surface-wave contributions for light scattering by homogeneous spheres and spheres with a shell structure [27]. In this development, we modified the ray-by-ray integration approach [28], which is particularly useful for the computation of extinction and absorption

cross sections for a particle composed of a spherical core surrounded by a concentric shell. This geometric-optics surface-wave theory for light scattering by spheres considers the surface-wave contribution as a perturbation term to the geometrics optics core that includes the Fresnel reflection–refraction and Fraunhofer diffraction. For surface-wave contributions, the analytical expressions derived for the terms involving the extinction and absorption cross sections and radiation pressure on the basis of the complex angular momentum theory [29] were followed. Reliability and accuracy of the geometric-optics surface-wave (*GOS*) approach have been assessed by comparison with the results determined from the Lorenz-Mie (*LM*) theory. The extinction efficiency, single-scattering albedo, and asymmetry factor results computed by *GOS* and *LM* are shown to be in close agreement for a combination of real-imaginary refractive indices as functions of size parameter [27].

The *GOS* approach has also been applied to spheres composed of a spherical core and a shell with a number of real and imaginary refractive indices and size combinations. The resulting computations were assessed with those evaluated from an efficient algorithm [30] based on the analytical *LM* solution for spherical core-shell structure. The same order of accuracy has been demonstrated as the cases involving homogeneous spheres. To simulate the core-shell structure of soot aerosols, we have extended the hit-and-miss Monte Carlo photon tracing program for homogenous particles [31,32] to concentrically stratified spheres [33]. The close agreement between *GOS* and the *"Exact" LM*-like solution provides the foundation to conduct physically reliable light absorption and scattering for aerosol aggregates with internal and external mixing, and closed- and open-cells, which can be built from homogeneous and concentric shell spheres with smooth and/or rough surfaces. Our objective is to demonstrate an attractive light scattering and absorption approach to complement existing methodologies cited above.

Accordingly, the present paper is organized as follows. In Section 2, we describe an approach to construct aggregates by means of stochastic processes. This is followed in Section 3 by the development of the *GOS* approach for nonspherical particles in general, and aggregates in particular. Verification of the *GOS* approach and pertinent computation results for light absorption and scattering by aggregates and snow grains with external and internal mixing configurations are discussed in Section 4. Concluding remarks are given in Section 5.

2. Construction of aggregates based on stochastic processes

In the present study, the particle that constitutes the building element of an aggregate has the following shape: a homogeneous sphere with smooth and irregular surfaces; and a sphere with core-shell structure in which the outer shell surface can be irregular, as shown in Fig. 1a. Surface irregularity can be imposed by perturbing the direction of the normal on surface of each sphere randomly when a light ray hits the surface. Specifically, the zenith angle ϑ_i and azimuthal angle φ_i of an individual normal to the light beam is perturbed stochastically from the original direction in the form: $\vartheta_i = \vartheta_m RN$ and $\varphi_i = 2\pi RN$, where the notation ϑ_m denotes a number smaller than $\pi/2$ and *RN* is a random number between 0 and 1. This approach followed the pioneering work developed by Cox and Munk [34] to represent the roughness of ocean surfaces.

For an aggregate model with a core-shell structure, we shall consider an aggregate consisting of n concentrically stratified spheres referred to as a "closed" aggregate [10,35], as shown in Fig. 1b. Each sphere has a core of an absorbing aerosol and a shell of a nonabsorbing aerosol. The shell radius r_{shell} is the same as the radius of a homogeneous sphere. The ratio of the core radius r_{core} to the shell radius r_{shell} is denoted by R, which ranges from 0 to 1. As stated above, irregularity can be introduced on the surface of aggregates; however, the inner boundary of a closed aggregate will be fixed as smooth for simplicity of analysis. There is another kind of internal mixture, referred to as "open" [36]. An open aggregate is defined by $(n-m)$ absorbing spheres (e.g. soot particles) surrounded by m nonabsorbing spheres (e.g. ammonium sulfate particles). The ratio of $n-m$ to m has been selected to make the volume and mass the same as closed aggregates for consistent comparison in light absorption and scattering calculations.

Aggregated aerosols are constructed stochastically following a procedure described by Friedlander [14] involving three kinds of agglomerate formation: ballistic aggregation (BA), diffusion-limited aggregation (DLA), and reaction-limited aggregation (RLA). For ballistic particle-cluster aggregation, a particle is first fixed at the origin, followed by injection of another particle from a point arbitrarily selected on a large sphere surrounding the origin, which proceeds along a straight line. If the latter hits the former, they are attached together; otherwise, the former particle moves away from the large sphere. This process is repeated until a desirable number of attached particles has been reached. In the case of diffusion-limited aggregation, an approaching particle undergoes a random walk instead of a straight path described above. Here random walk implies that a series of sequential movements in which the direction of each move is randomly determined as follows:

$$x_i' = x_i + 2\sqrt{2}(RN - 1/2), \quad i = x, y, z \tag{1}$$

where x_i is a position, x_i' is a subsequent position, and *RN* is a random number from 0 to 1. The RLA particle is similar to DLA; however, it requires repeated collisions before cohering. In the following study, we shall confine our efforts to BA and DLA in association with light scattering and absorption calculations due to the similarity of RLA to BA. After Mandelbrot [37], fractal (Hausdorff) dimension D_f can be expressed as follows:

$$n \propto r_g^{D_f} \tag{2}$$

where n is the number of spherules in an aggregate and r_g, the aggregate radius of gyration, is defined by

$$r_g^2 = \frac{1}{n}\sum_{i=1}^{n} |\mathbf{r}_i - \mathbf{r}_0|^2 \tag{3}$$

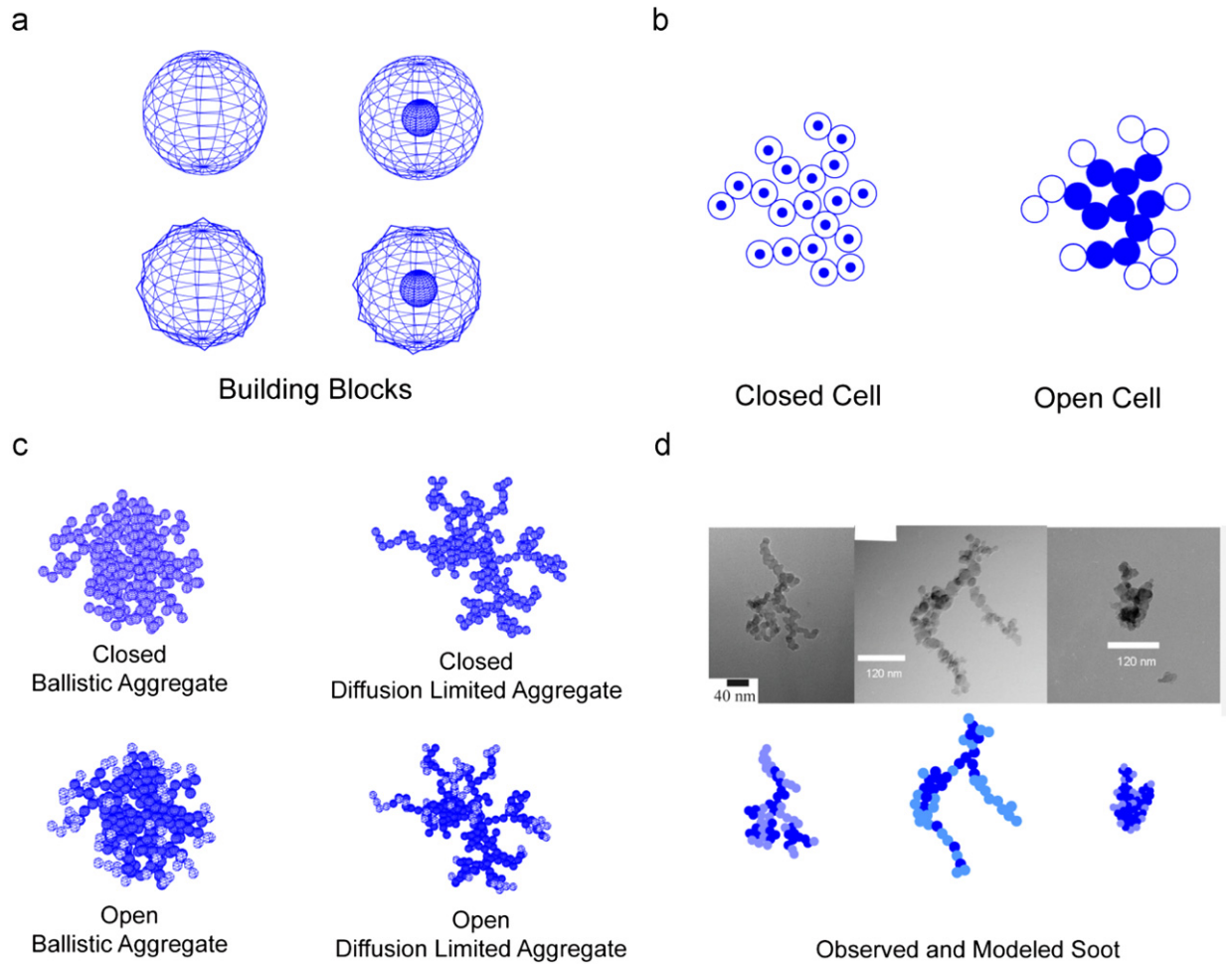

Fig. 1. Illustration of the morphology and composition of aggregates: (a) basic building blocks, including homogeneous or shell-core spheres with smooth and/or rough surfaces; (b) definitions of open- and closed-cells; (c) definitions of ballistic and diffusion-limited aggregates constructed by means of stochastic procedures (see text for further explanation); and (d) observed soot particles in the air and computer generated models. (For interpretation of the references to color in this figure, the reader is referred to the web version of this article.)

where $\mathbf{r}_0$ is the position of center of mass given by

$$\mathbf{r}_0 = \frac{1}{n}\sum_{i=1}^{n}\mathbf{r}_i \tag{4}$$

Based on the preceding definitions, BA and DLA aggregates, as illustrated in Fig. 1c have fractal dimensions of 2.45 and 2.27, respectively.

Shown in Fig. 1d is a chain aggregate soot particle, referred to as "cat in the hat" [14], collected from ambient air on the UCLA campus. The corresponding computer modeled aggregates are displayed below in blue. Once the shape and composition are defined, we can carry out light absorption and scattering calculations accordingly. However, it is not clear whether these particles are associated with the state of open- or closed-cells. Our modeling efforts are in line with the observations presented by Martins et al. [10], (Fig. 5). The present closed-cell model presented in Fig. 1c mimics those presented by Strawa et al. [35], (Fig. 1), while the open-cell aggregate structure shown in that figure is similar to the coated soot particles generated by Stratmann et al. [36], (Fig. 4). Furthermore, Jacobson [11] discussed cases involving "high shell/core ratio" and "low shell/core ratio" as possible "models."

3. Light absorption and scattering by aggregates: A geometric-optics surface-wave approach

3.1. Geometric optics

Fig. 2 illustrates the geometric optics (reflection/refraction and diffraction) and surface-wave approach applied to a group of shell spheres, which form an aggregate. The geometric reflection and refraction can be carried out using the hit-and-miss Monte Carlo photon tracing once the shape and composition of an aggregate are defined from the stochastic processes described in Section 2. Following the ray-by-ray integration approach [27,28], the extinction and absorption cross sections for a single

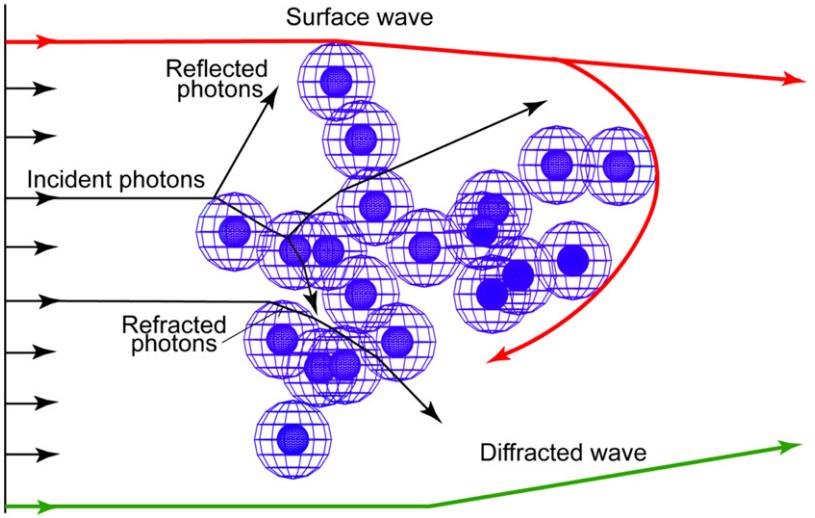

Fig. 2. Graphical depiction of the geometric optics and surface waves approach for light scattering by an ensemble of shelled spheres (aggregate). The geometric optics components include the hit-and-miss Monte Carlo photon tracing associated with external and internal reflections and refractions, and diffraction based on Babinet's optical principle for randomly oriented nonspherical particles. The surface waves travel along the edge of the particles and propagate into shadow regions.

aggregate are defined by

$$\sigma_e = \frac{2\pi}{k^2}\mathrm{Re}\left[S_{11}(\hat{e}_0)+S_{22}(\hat{e}_0)\right] \tag{5}$$

$$\sigma_a = \frac{1}{2}\sum_{\gamma}\sum_{p=1}^{\infty}\exp\left(-2k\sum_{j=1}^{p-1}m_{i,j}d_j\right)\left[1-\exp(-2km_{i,p}d_p)\right]\left(t_1^2r_1^{p-1}+t_2^2r_2^{p-1}\right) \tag{6}$$

where k is the wavenumber, Re denotes the real part, S_{11} and S_{22} are two diagonal elements of the scattering amplitude matrix in the forward direction, $\hat{e}_0$ denotes the incident direction, the subscript index $p(=1,2,3,\ldots)$ denotes the internal localized ray, γ in the first summation of the absorption cross section covers all incident photons impinging onto the sphere, $m_{i,j(or\ p)}$ represents the imaginary part of the refractive index for an inhomogeneous sphere, $d_{j(or\ p)}$ is a vector distance between two points, and $t_j^2r_j^{p-1}(j=1,\ 2)$ denotes the cumulative product of Fresnel coefficients.

We shall now consider a group of aggregates in space. In view of their irregular shape and small size, three-dimensional random orientation appears to be an excellent assumption for light absorption and scattering studies. Under this condition, we may then define an effective geometric cross section area to evaluate the extinction and absorption efficiencies. For this purpose, let A be the area of a square, which is sufficiently large to cover the geometric cross section of an aggregate, and set this square equal to L^2, where L denotes the particle's maximum dimension. Further, let N_a be the number of photons incident on aggregates, which is dependent on the particle's orientation, and N_t be the number of total photons used in the calculation. Thus, the effective geometric shadow of an aggregate on a plane perpendicular to the incident light beam, whose propagation direction is along the z-axis, can be defined as follows:

$$A_s(\alpha,\beta) = A[N_a(\alpha,\beta)/N_t] \tag{7}$$

where α and β are angles, which denote the orientation of an aggregate in a two-dimensional plane with reference to the incident light beam. It follows that for an ensemble of randomly oriented aggregates, the extinction and absorption efficiencies averaged over all orientations can be written in the form

$$Q_{ext,abs} = \int_{\alpha}\int_{\beta}\sigma_{e,a}(\alpha,\beta)\cos\alpha\,d\alpha\,d\beta \Big/ \int_{\alpha}\int_{\beta}A_s(\alpha,\beta)\cos\alpha\,d\alpha\,d\beta. \tag{8}$$

Next, we shall discuss the diffraction component for aggregates. The original theoretical development of diffraction begins with Babinet's principle, which states that the diffraction pattern in the far field (Fraunhofer diffraction) from a circular aperture is the same as that from an opaque disk or sphere of the same radius. Following this principle and in order to apply it to randomly oriented nonspherical particles, we may use the effective geometric cross section area defined in Eq. (7). Thus, the diffracted intensity I_d for an ensemble of randomly oriented aggregates can be expressed by [38,39]

$$I_d \propto \int_{\alpha}\int_{\beta}\left|\iint_{A_s}\exp\left[-ikr(x,y,\alpha,\beta)dxdy\right]\right|^2\cos\alpha\,d\alpha\,d\beta \tag{9}$$

where r is the distance between a point in the shadow A_s and a distant point from the shadow. Analytical solutions for Eq. (9) exist only for simple nonspherical shapes, such as column, plate, and spheroid [31,32,40]. However, "exact" numerical calculations can be carried out for irregular particles such as aggregates to obtain the diffracted energy.

On the basis of the scattered intensities determined from geometric reflection and refraction and diffraction

for randomly oriented aggregates, the asymmetry factor g can be determined. Subsequently, we can evaluate the term referred to as radiation pressure efficiency [27,41], the concept of which can be applied to nonspherical particles as follows:

$$Q_{pr}(GO) = Q_{ext}(GO) - g(GO)[Q_{ext}(GO) - Q_{abs}(GO)] \quad (10)$$

where the symbol GO stands for geometric optics and Q_{ext} and Q_{abs} have been defined in Eq. (8).

3.2. Surface waves

Surface waves in the context of light scattering and absorption by a sphere are generated by interactions of the incident waves at the grazing angles near the sphere's edge and propagate along its surface into the shadow region [29,41]. On the basis of theoretical postulations and numerical calculations, Liou et al. [27] demonstrated that a linear combination of the geometric optics term (reflection/refraction and diffraction, denoted by GO) and the surface-wave adjustment (denoted by GOS) constitutes a solution close to the exact Lorenz–Mie theory (denoted by LM) so that

$$Q_w(GOS) = Q_w(GO) + f\Delta Q_w \sim Q_w(LM),\ w = ext,\ abs,\ pr \quad (11)$$

where Q_w is the efficiency factors for extinction (ext), absorption (abs), or radiation pressure (pr), ΔQ_w is the surface-wave adjustment, and a parameter f has been inserted into this equation. In our previous analysis for spheres, we set $f=1$. However, for large size parameters greater than about 50, f is close to 0. Once Q_{pr} has been determined, the asymmetry factor from Eq. (10) associated with GOS can be written in the form

$$g(GOS) = \left[1 - Q_{pr}(GOS)/Q_{ext}(GOS)\right]/\varpi(GOS) \quad (12)$$

where the single-scattering albedo ϖ is defined by Q_{sca}/Q_{ext} and $Q_{sca} = Q_{ext} - Q_{abs}$.

Surface waves differ from diffraction, which originates from the incomplete wave front due to the blocking of the incident wave by the scattering particle and is governed by the geometric cross section area facing the incident light beam. However, surface waves propagate along the particle's surface and hence must be associated with light absorption in addition to scattering. The theoretical foundation for surface waves exists only for spheres as discussed previously. For nonspherical particles, a physically based adjustment must be developed in order to effectively account for the factor of shape. Irregular surfaces will suppress the propagation of these waves and reduce the effectiveness of their interactions with the particle, slow down the waves so to speak. Spheres, by virtue of smooth surfaces, are the most efficient geometry for wave propagation. Thus, the parameter introduced in Eq. (11) must be less than 1 for nonspherical particles: i.e., it is close to zero for an elongated particle since the probabilities for the forward and backward propagations of surface waves would be limited in this case. Volume (three-dimensional) must also play a key role in the effectiveness of surface-wave contributions.

Two types of volume can be defined. We may define a volume for an aggregate as follows:

$$V_v = n \times 4\pi r_v^3/3 \quad (13)$$

where r_v is the radius of a sphere used to build an aggregate and n is the total number of spheres. We may also define a volume corresponding to the geometric cross section area, A_s, defined in Eq. (7) such that

$$V_a = n \times 4\pi r_a^3/3 \quad (14)$$

where $\pi r_a^2 = A_s$. We postulate that the correction parameter in Eq. (11) for nonspherical particles may be defined by the ratio of two volumes as follows:

$$f = V_v/V_a = (r_v/r_a)^3. \quad (15)$$

We find that V_v (or r_v) is smaller than V_a (r_a) so that f is equal to or less than 1. For spheres, $r_v = r_a$, so that $f=1$; for elongated particles, $r_v \ll r_a$ so that $f \sim 0$. These limits provide a theoretical basis and boundary conditions for the application of Eq. (11) to nonspherical particles.

4. Computational results and discussion

We first conduct a comparison of the preceding theoretical developments for application to nonspherical columns and plates to those determined from the Finite Difference Time Domain (FDTD) method pioneered by Yee [42] and later employed by Yang and Liou [43] to study the light scattering and absorption properties of nonspherical ice crystals. Yang et al. [44] carried out comprehensive computations employing FDTD and a modified and improved geometric optics method [45] for a number of ice crystal shapes and sizes covering a spectrum of wavelengths, and provided a database for application to remote sensing and radiative transfer. We also compare our present results to those computed from the Discrete Dipole Approximation (DDA) method originally developed by Purcell and Pennypacker [46] and later by Draine and Flatau [47] in which the single-scattering results for small size parameters for column and plate can be computed from existing programs [48]. DDA calculates light scattering and absorption by a target with arbitrary geometry in which the target is defined by an array of discrete dipoles located on a cubic lattice. Both the FDTD and DDA methods require a tremendous amount of computational effort for moderate size parameters, particularly when the 3D orientation of nonspherical particles is accounted for in the computations. For this reason, it is quite challenging to employ FDTD and DDA for many practical applications involving nonspherical particles with size parameters larger than about 20.

We have selected two wavelengths for comparison purposes: 3.7 and 23 μm with refractive indices for ice of $1.4005 - i0.007201$ and $1.4424 - i0.02701$, respectively [44]. Fig. 3 illustrates a comparison of the single-scattering parameters (extinction efficiency, single-scattering albedo, and asymmetry factor) for randomly oriented columns (a) and plates (b) as a function of size parameter defined as $x_{max} = kr_{max} (= L_{max}/2)$, where L_{max} denotes the maximum dimension and k is the wavenumber. Because of their computational limitations, FDTD and DDA results are shown for size parameters less than about 20. For column, GOS results compare closely with values computed from FDTD and DDA for both wavelengths (3.7 and 23 μm) for the three single-scattering parameters. We note that GOS results show slight systematic overestimations in the extinction

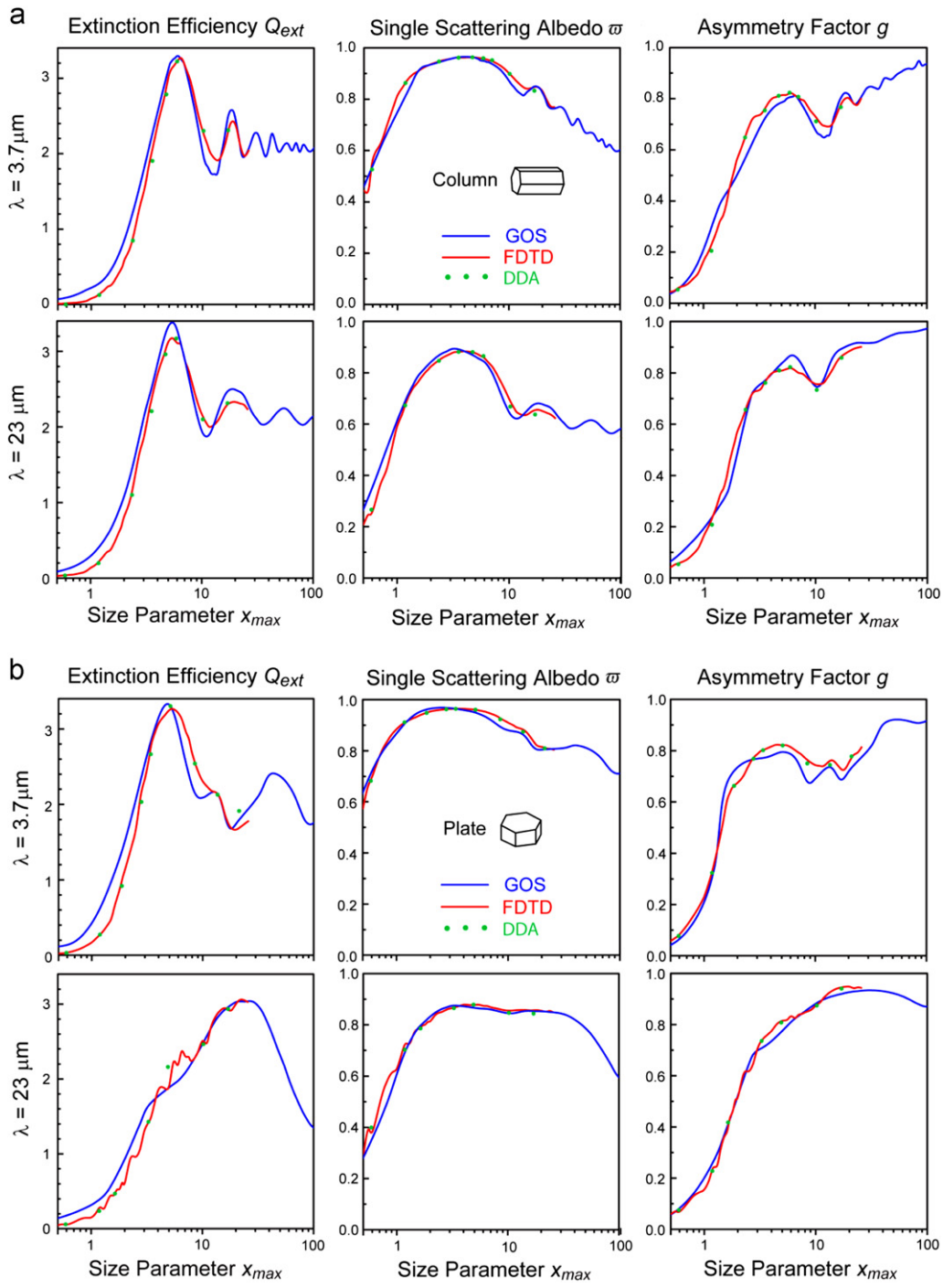

Fig. 3. Comparison of the single-scattering parameters (extinction efficiency, single-scattering albedo, and asymmetry factor) for randomly oriented columns (a) and plates (b) as a function of size parameter x_{max}, which is defined as $2\pi r_{max}/\lambda$, where r_{max} denotes one half of the maximum dimension and λ is the wavelength, computed from the geometric optics and surface-wave approach (*GOS*) for size parameters up to 100, and from the finite-difference time domain (FDTD) and the discrete dipole approximation (DDA) computer codes for size parameters smaller than about 20.

efficiency for size parameters smaller than about 2–3. For plate, *GOS* results compare closely with values calculated from FDTD and DDA for single-scattering albedo as well as asymmetry factor. Some deviations are shown in the extinction efficiency curves; in particular, the *GOS* approach, which is a linear combination of geometric optics and surface waves, does not depict the fluctuations produced in FDTD results in the case of 23 µm. In addition to the preceding comparisons, we have made an effort to compare with pertinent results presented in Liu et al. [26]. For

illustrative purposes, we selected a case involving a homogeneous sphere aggregate with $m=2-i1$, $n=200$, $D_f=2.46$, $a=0.015\ \mu m$, and $\lambda=0.87\ \mu m$ based on the results presented in their Table 2 and Fig. 2. Following *GOS* and using these parameters as input, we conducted computations for extinction and absorption cross sections and asymmetry factor, and obtained $C_{ext}=0.0518\ \mu m^2$, $C_{abs}=0.0318\ \mu m^2$, and $g=0.143$. Compared with Liu et al.'s values of $C_{ext}=0.0287\ \mu m^2$, $C_{abs}=0.0245\ \mu m^2$, and $g=0.177$, some differences are noted, which could be due, in part, to the aggregate shape generated from our stochastic processes denoted in Section 2. Also, as noted for the column case above, *GOS* results depicted slight systematic overestimations in the extinction efficiency for size parameters smaller than about 2.

The preceding comparisons were intended to check the applicability of the new theoretical development (*GOS*) for light scattering and absorption by nonspherical particles, which is computationally efficient and can be readily applied to a spectrum of size parameters and irregular shapes such as aggregates, complementary to existing methodologies. In what follows, we present a number of sample calculations to demonstrate *GOS*'s applicability to aggregates and snow grains.

Fig. 4 shows the extinction efficiency Q_{ext}, the single-scattering albedo ϖ, and the asymmetry factor g as a function of size parameter x_{max} defined previously. In these calculations, 256 (arbitrarily selected) rough-surface spheres were used to build aggregates. For the case of closed-cell, each building sphere contained a 90% soot core with a refractive index of $2-i1$ [22], coated by a 10% shell layer of nonabsorbing ammonium sulfate with $m=1.53$. For the case of open-cell, 187 were soot and 69 were sulfate particles, such that the volume and mass of the total building spheres were the same. This ratio is close to the configuration presented in Martins et al. [10]. For the former, which consists of internally mixed spheres, the two types of aggregates (BA and DLA) were constructed following the stochastic procedure described in Section 2. For the latter, the 187 soot spheres were first constructed stochastically as a core, followed by 69 ammonium sulfate spheres, which were located outside of this core. These aggregate models correspond to the "low shell/core ratio" internal mixing discussed by Jacobson [11].

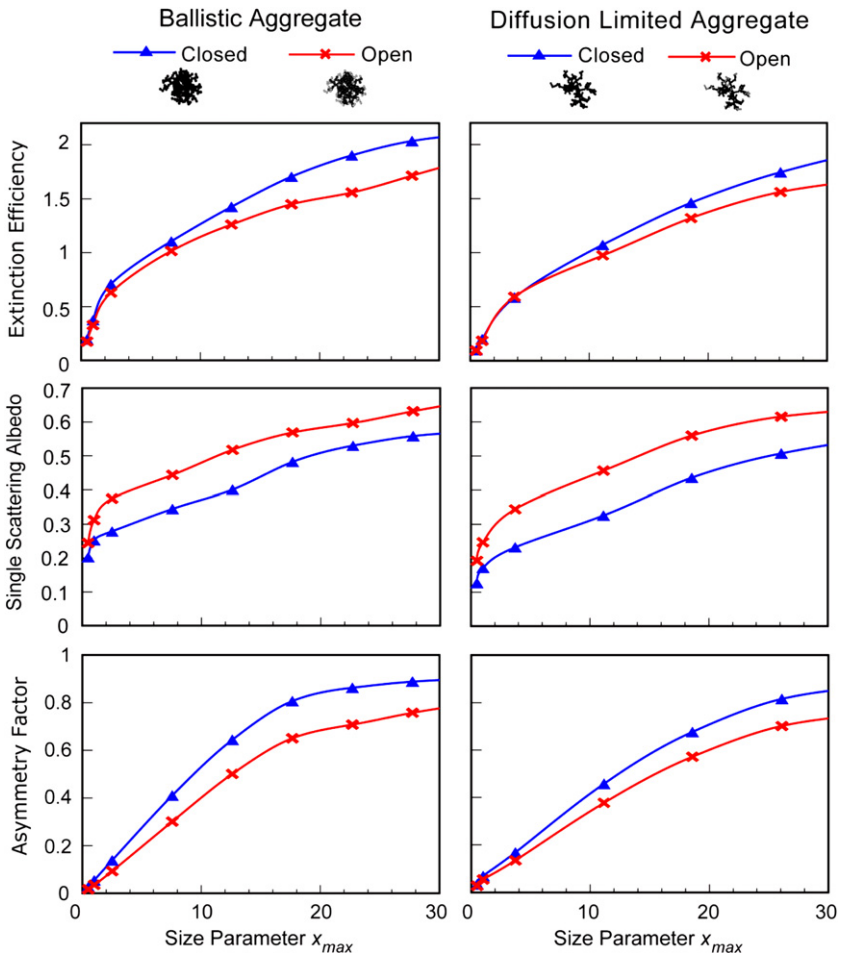

Fig. 4. Extinction efficiency Q_{ext}, the single-scattering albedo ϖ, and the asymmetry factor g for a group of randomly oriented aggregates (Ballistic and Diffusion Limited) in terms of open- and closed-cell configurations as a function of x_{max} using a wavelength of 0.67 μm in the calculations. The size parameter $x_{max}=2\pi r_{max}/\lambda$, where r_{max} is half of the particle maximum dimension and λ is the wavelength.

For the same volume and mass, closed-cell cases (internally mixed spheres) have larger absorption (smaller single-scattering albedo, second panel) than their open-cell counterparts with differences on the order of 10–15%. Due to stronger absorption, most of the scattered energy for closed-cell cases is confined to forward directions, leading to larger asymmetry factors, as shown in the bottom panel. Under the condition of the same volume and mass, the extinction efficiencies for closed-cell cases are larger than the open-cell counterparts associated with larger absorption and stronger forward scattering. Also, DLA absorbs and scatters slightly more than BA because of a larger geometrical cross section.

Another parameter of interest is specific absorption α_a, defined as the absorption cross section per unit mass, which can be measured in laboratory [22,49,50]. It is given by

$$\alpha_a = \sigma_a / M = \frac{A_s Q_{abs}}{\sum_i \rho_i V_i} \tag{16}$$

where σ_a is the absorption cross section, M is the mass, A_s is the average geometric cross section defined in Eq. (7), Q_{abs} is the absorption efficiency, ρ_i is the density, and V_i is the volume. The summation over i covers the inhomogeneous part of spherule if applicable. We used $\rho_{sulf} = 1$ g/cm^3 in the calculations. Also, two values of the refractive indices were used for soot: $2-i1$ ($\rho_{soot}\sim 2$ g/cm^3) and $1.75-i0.75$ ($\rho_{soot}\sim 1.8$ g/cm^3), representing upper and lower limits respectively [22]. These are very close to the best value of $1.95-i0.79$ recommended by Bond and Bergstrom [49], (p. 47 and Fig. 7). Our absorption and scattering calculation results using this value are within the range of the preceding values.

Fig. 5 depicts specific absorption as a function of size parameter x_{max}, derived from the extinction efficiency and single-scattering albedo values displayed in Fig. 4. The specific absorption for DLA is greater than that for BA because the average geometric cross sectional area for the former is larger than that for the latter when volume and mass are kept the same. Also, the specific absorption for closed aggregates is larger than that for open aggregates corresponding to differences in the single-scattering albedo shown in Fig. 4. Sheridan et al. [51] conducted a comprehensive evaluation of the aerosol absorption measurement techniques and found that the specific absorption at a wavelength of 0.53 μm for pure kerosene soot with a mode radius of 0.15 μm has a value of 7.5 ± 1.2 m^2/g. This error bar appears to be in line with that presented in Bond and Bergstrom [49]. The compositions associated with absorption measurements appear to be largely externally mixed ammonium sulfate and kerosene soot aerosols that were collected during the experiments. We have placed the measured values (circles with error bar) along with our computational results for BA and DLA associated with open- and closed-cell conditions, and demonstrated the compatibility of theoretical results and measured values. For size parameters larger than 10, the dependence of specific absorption on the refractive indices selected in this study become less significant,

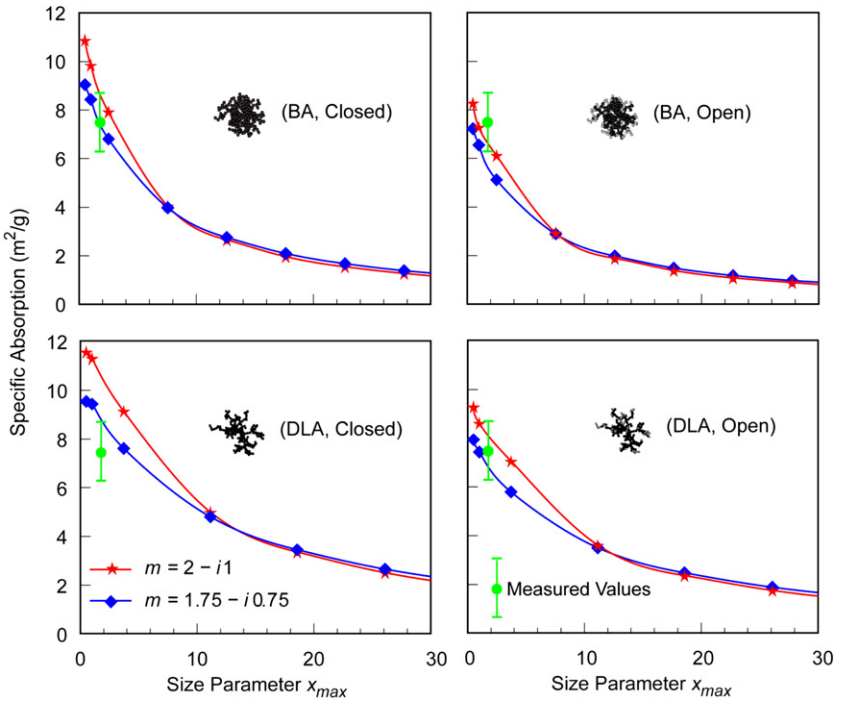

Fig. 5. Specific absorption (m^2/g) for two types of aggregates (Ballistic, BA; and Diffusion Limited, DLA) for closed- and open-cell configurations. The upper and lower limits for the refractive indices of soot used in the calculations are also shown in the figure. Also depicted in the figure are laboratory measured values in terms of mean and standard deviation presented by Sheridan et al. [51].

because photons travel within aggregates are substantially absorbed due to longer path and intense absorption. Also, we compared specific absorption values with those presented by Liu et al. [26], who used the superposition T-matrix method to evaluate the absorption cross section for aggregates discussed previously. Using their Table 2, we obtained upper limits for α_a of 3.5 and 4.3 (m^2/g) for the case of $m=1.75-i0.5$ and $2-i1$, respectively. These values do not vary significantly with aggregate size. We fully realize that a more comprehensive and careful comparison between theoretical and experimental results is a subject for further investigation and would require the size, shape, and composition information for direct input into the light absorption and scattering program.

To study the absorption and scattering properties of internal and external mixtures for aerosols, spheres were used and the radii of core and shell spheres for internal mixture were defined as r_{soot} and r_{sulf}, respectively. For external mixture, the radii of core and shell spheres are denoted as r_{soot^*} and r_{sulf^*}. In this study, we used the index of refraction of $2-i1$ in the calculations. Two external mixings are shown in Fig. 6: Soot is on the surface of the nonabsorbing sulfate (Case 1) or some distance away from it (Case 2). The *GOS* results of the single-scattering properties (extinction efficiency, single-scattering co-albedo, and asymmetry factor) for the two cases are essentially the same based on our theoretical calculations (Fig. 6). For this reason, we shall select Case 2 to compare with internal mixing results. In order to have a physically-based comparison, we have made the same volume and mass for the two configurations. Fig. 6 depicts the three single-scattering properties as a function of r_{sulf} (keeping $r_{soot}/r_{sulf}=0.1$, left panel) and r_{soot} (keeping $r_{sulf}=10\,\mu m$, right panel). The extinction efficiency and asymmetry factor values are very similar for external and internal mixings because the contributions of diffraction and surface waves are about the same for the two configurations. However, the single-scattering co-albedo for internal mixing displays a factor of 2.55 greater than that for external mixing, principally due to the trapping of photons within the particle.

In the following, we investigate the effect of absorbing aerosols on single-scattering properties associated with external and internal mixing. Three shapes were used in this investigation: sphere, plate, and plate with rough surfaces. The spherical ice particle has a radius of 50 μm, while randomly oriented pristine and rough-surface plates have the same cross section area. The top panel of Fig. 7 illustrates the shape effect on the single-scattering co-albedo and asymmetry factor for pure ice using the 0.55 μm wavelength. Although the shape effect is not significant in terms of single-scattering co-albedo, its effect on the asymmetry factor g is substantial. The pure spherical ice scatters much more light in forward directions with a g value of about 0.89, whereas the g value reduces to 0.81 for the case involving plate with rough surfaces. The irregular plate has a noticeable smaller value as compared to the pristine plate, caused by the reduction in forward diffraction. The middle and bottom panels show the effects of external and internal mixing states, respectively, on the absorption and scattering properties of snowflakes. As illustrated in the middle-left panel, the single-scattering co-albedo ($1-\varpi$) ($=C_{abs}/C_{ext}$) for external mixture is proportional to r_{soot}^2 or the soot's geometric cross section area. The numerator C_{abs} is approximately given by $(1-\varpi)\times 2\pi r_{soot}^2$, while the denominator C_{ext} is close to a constant value of $2\pi\times(50\,\mu m)^2$. Thus, if we express $(1-\varpi)$ as a function of r_{soot}^2, it has a constant value of about 0.3696. Compared to external mixing, the single-scattering co-albedo for internal mixing (bottom-left panel) is enhanced by a factor of $\sim$1.9 with a slight dependence on snowflake shape. For the asymmetry factor, the results for external and internal mixings, shown in the middle and bottom panels, are similar to those presented in the top panel: i.e., the forward scattering nature of these particle configurations remains about the same.

Lastly, we study the effect of external and internal mixings on snow albedo. We presented the cases for soot aggregates and dust particles by employing a wavelength of 0.55 μm and the cosine of the solar zenith angle μ_0 of 0.5 in the calculations. The top panel of Fig. 8 shows the single-scattering co-albedo for three snow grains (represented by snowflakes) of 50 μm radius contaminated by soot (r_{soot}) or dust (r_{dust}) with radii ranging from 0.1 to 5 μm. As illustrated in Fig. 7, the asymmetry factor values for the three irregular shapes are very close. In radiative transfer calculations, we assume that the snow layer is semi-infinite and homogeneous and that the independent scattering concept may be applied since in general the distances between snow grains are much larger than visible wavelengths [52,53]. We follow the adding/doubling principle for radiative transfer in which the phase function is expressed in terms of the Henyey–Greenstein function defined by the asymmetry factor g as follows:

$$P_{HG}(\cos\Theta)=(1-g^2)/(1+g^2-2g\cos\Theta)^{3/2}. \tag{17}$$

The lower panel shows the snow albedo defined by the ratio of the reflected (diffuse) solar flux and the incident solar flux both at the top of a snow layer as follows [31]:

$$r(\mu_0)=\frac{F_{dif}^{\uparrow}(0)}{\mu_0 F_{\odot}}=\frac{1}{\pi}\int_0^{2\pi}\int_0^1 R(\mu,\phi;\mu_0,\phi_0)\mu\,d\mu\,d\phi \tag{18}$$

where R is the bidirectional reflection function expressed in terms of the cosine of the zenith angle μ and azimuthal angle φ. The albedo of pure snow is about 0.98. In the cases of external and internal mixings, snow albedo reduces to 0.97 and 0.95, respectively, for r_{soot} of 0.1 μm. However, an r_{soot} of 1 μm in the internal mixing case is shown to reduce the snow albedo to 0.9. The reduction of snow albedo is smaller for dust particles due to their weaker absorption. It is clear that repeated wet and dry depositions involving black carbon and dust would substantially darken the snow layer.

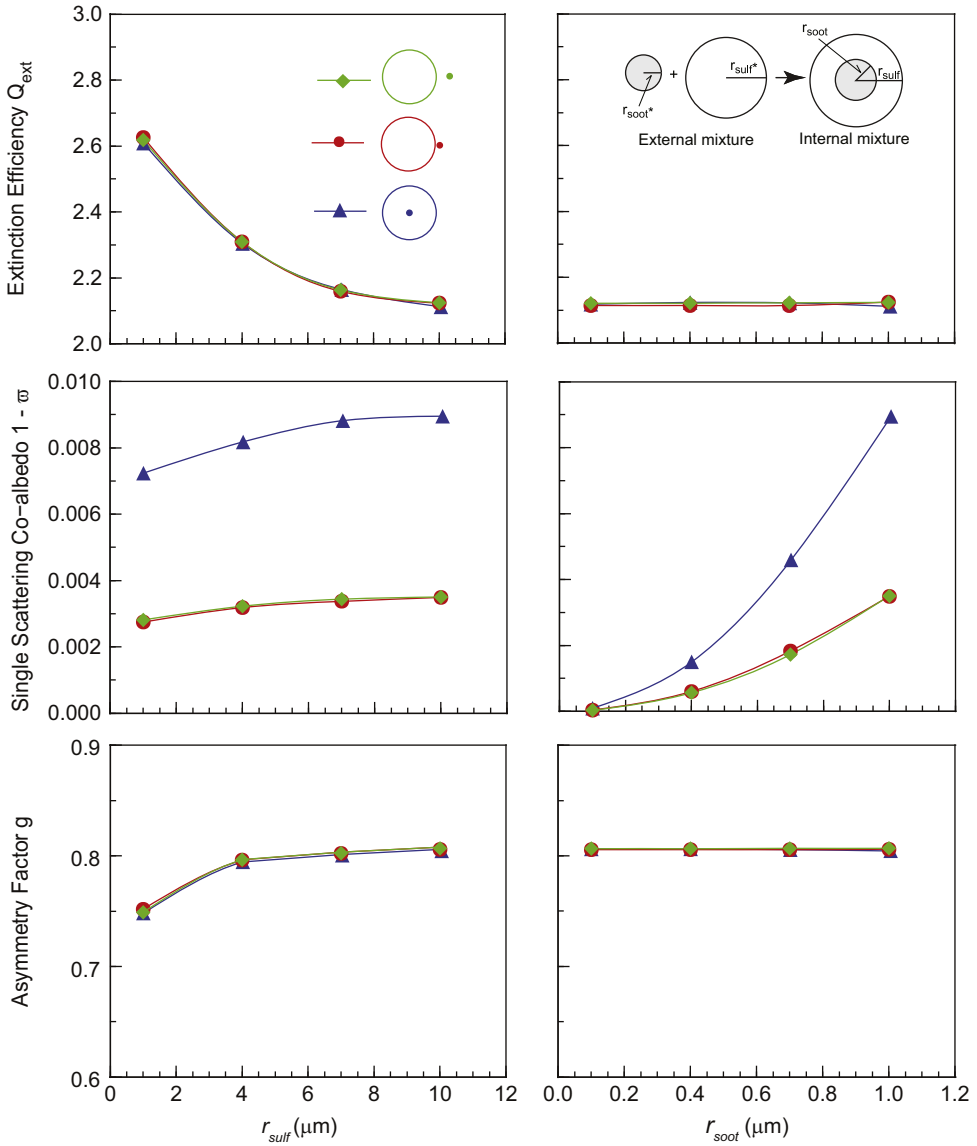

Fig. 6. Extinction efficiency Q_{ext}, the single-scattering co-albedo $(1-\varpi)$, and the asymmetry factor g for an ammonium sulfate aerosol (r_{sulf}) containing a soot core (r_{soot}) first as a function of r_{sulf} keeping $r_{soot}/r_{sulf}=0.1$ (left panel), and secondly as a function of r_{soot} keeping $r_{sulf}=10$ μm (right panel). There are three types of mixtures: external mixture (top), quasi-external mixture (middle), and internal mixture (bottom), as shown in the top-left panel. Also inset in the top-right panel are the definitions of radii r_{soot^*} and r_{sulf^*} of core and shell spheres for external mixtures.

5. Concluding remarks

We have developed a geometric-optics surface-wave approach for the computation of light absorption and scattering by nonspherical particles for application to aggregates and snow grains with external and internal mixing structures. Aggregates are formed by stochastic procedures using homogeneous and core-shell spheres, which can be composed of smooth or rough surfaces, as building blocks. In the theoretical development, we followed the concept of adding the surface-wave contribution as a perturbation term to the geometric optics core, including Fresnel reflection–refraction and Fraunhofer diffraction. In the reflection and refraction components, the complex aggregate shape and composition can be accounted for by using the hit-and-miss Monte Carlo photon tracing method. We followed Babinet's principle for diffraction in the far field in a 2D domain and developed an integral expression for diffraction by randomly oriented aggregates based on a weighted geometric cross section, which takes into accounts the number of photons impinging on the particle. With reference to surface waves, a nonspherical correction factor was introduced using a non-dimensional volume parameter such that the wave contribution is 1 for spheres and ~0 for elongated particles. We performed comparison of the single-scattering results, including extinction efficiency, single-scattering albedo, and

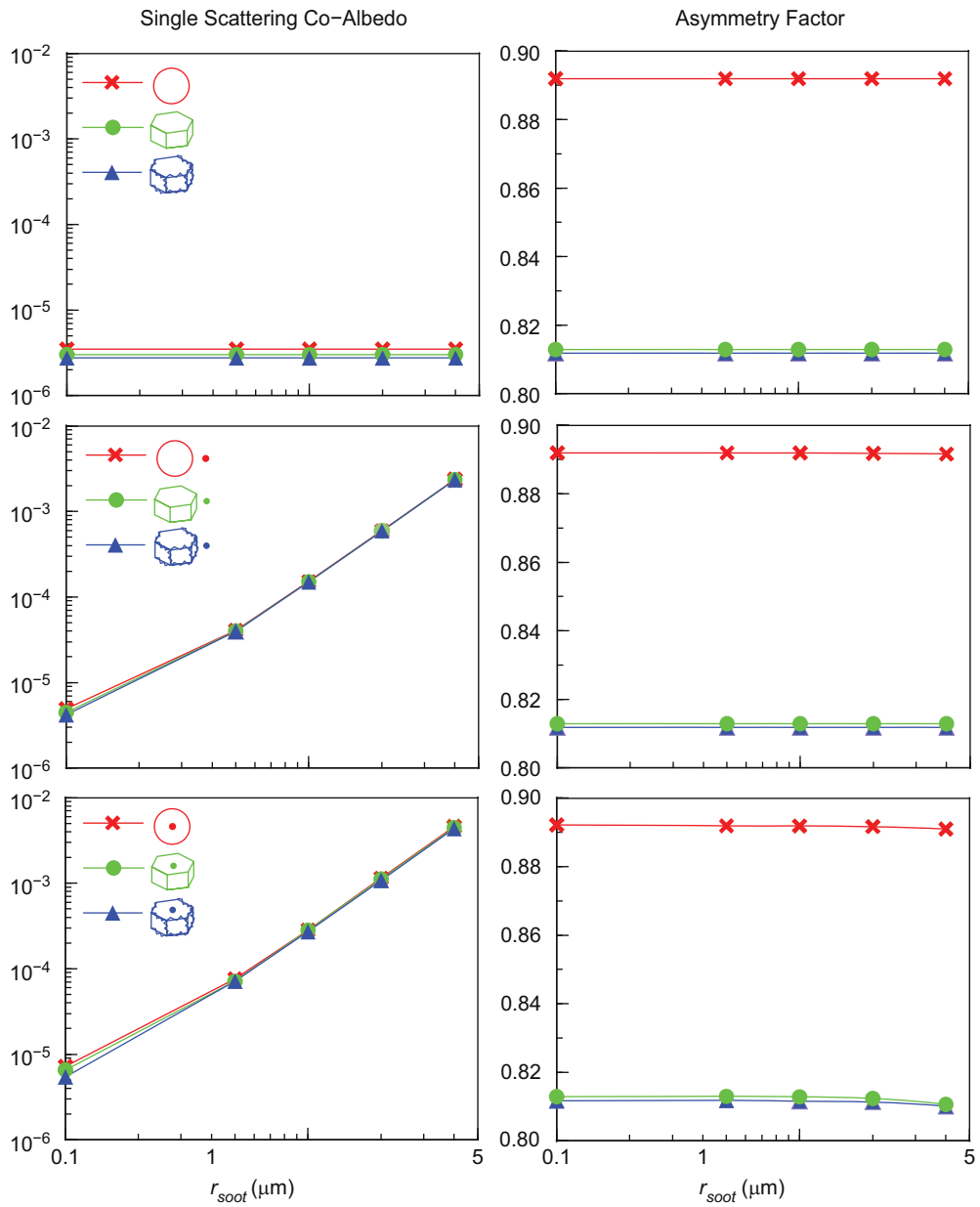

Fig. 7. Single-scattering co-albedo ($1-\varpi$) and the asymmetry factor as a function of soot radius r_{soot} for a sphere, a pristine plate, and a plate with rough surfaces with a radius of 50 μm, representing snow grains. The top, middle, and bottom panels are for pure, externally mixed, and internally mixed snow grains computed from *GOS* using a wavelength of 0.55 μm.

asymmetry factor, for light scattering by columns and plates for which the results computed from the FDTD and DDA methods can be used for cross checking.

We demonstrated that the extinction efficiency, the single-scattering albedo, and the asymmetry factor for randomly oriented columns and plates as a function of size parameter evaluated from the geometric-optics and surface-wave theory are comparable to the results derived from the FDTD and DDA counterparts for size parameters smaller than about 20, beyond which the rigorous numerical approaches are computationally unfeasible. The present theoretical approach covers all size ranges and is particularly attractive from the perspective of treating light absorption and scattering by complex particle shapes and inhomogeneous compositions.

Application of the geometric-optics and surface-wave approach was performed with reference to a number of aggregate configurations generated by stochastic procedures, including ballistic and diffusion-limited aggregates with closed and open configurations (see Fig. 1). We showed that under the condition of equal volume and mass, closed-cell cases have larger absorption than their open-cell counterparts for both BA and DLA. Owing to stronger absorption in closed-cell cases, most of the

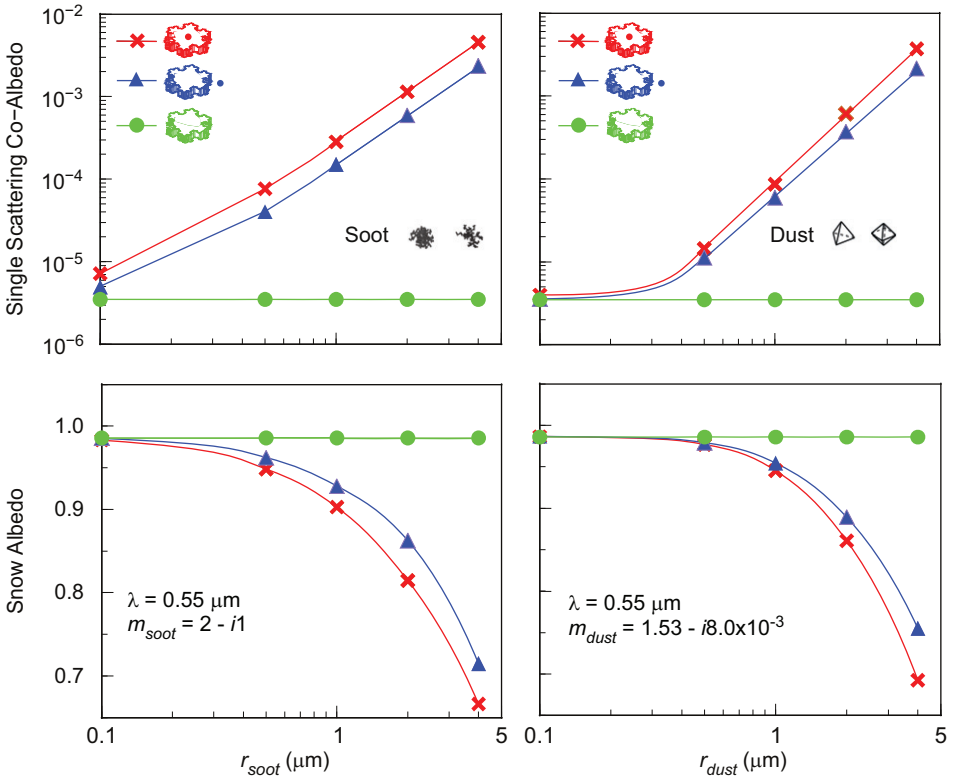

Fig. 8. Upper panel shows the single-scattering co-albedo for three types of snowflakes (pure, externally mixed, and internally mixed) with a radius (half of the maximum dimension) of 50 μm as a function of r_{soot} or r_{dust} ranging from 0.1 to 4 μm. The refractive indices for soot and dust and the wavelength used in the calculations are depicted in the figure. The lower panel shows the corresponding results for snow albedo for a cosine of the solar zenith angle of 0.5. The snow layer is assumed to be optically semi-infinite and homogeneous in radiative transfer calculations using the adding/doubling method (see text for further explanation).

scattered energy is confined to forward directions, leading to a larger asymmetry factor than open-cell cases. Attempts were also made to compare computed specific absorption results with those determined from laboratory experiments for homogeneous aggregates based on photoacoustic techniques. However, it is clear that much work still needs to be done regarding closure comparison for case studies using measured size, shape and composition for input to theoretical models. Nevertheless, we have illustrated compatibility between theoretical results and measured values.

The effects of particle shape on internal and external mixing were investigated employing sphere, plate, and plate with rough surfaces. Light absorption for randomly oriented plates is close to that of the spherical counterpart under the condition of equal geometrical cross section for both external and internal mixing states. However, plates scatter less light in forward directions than spheres resulting in a reduction by about 9% in the asymmetry factor. We further studied the effects of internal and external mixing of soot and dust particles associated with snowflakes on snow albedo. In this quest, we used an adding/doubling radiative transfer program for an infinite, homogeneous snow layer to evaluate its albedo and demonstrated that an internally mixed small soot and dust particle of the order of 1 μm could effectively reduce snow albedo by as much as 5–10%. Indeed, the dry and wet depositions of black carbon and dust particles would substantially reduce the albedo of mountain snow (i.e. it would become darker), leading to surface warming and snowmelt, providing the effective positive feedback, and amplifying regional climatic surface temperature warming.

Acknowledgments

The research work presented in this paper was supported by the National Science Foundation under Grant AGS-0946315. We thank Suzanne Paulson for providing the observed soot samples depicted in Fig. 1(d), and Patrick Arnott for a helpful discussion on the measurements of specific absorption for soot particles.

References

[1] Menon S, Hansen JE, Nazarenko L, Luo Y. Climate effects of black carbon aerosols in China and India. Science 2002;297:2250–3.
[2] Gu Y, Liou KN, Chen W, Liao H. Direct climate effect of black carbon in China and its impact on dust storms. J Geophys Res 2010;115: D00K14, doi:10.1029/2009JD013427.

[3] Jacobson MZ. Strong radiative heating due to the mixing state of black carbon in atmospheric aerosols. Nature 2001;409:695–7.
[4] Ramanathan V, Carmichael G. Global and regional climate changes due to black carbon. Nat Geosci 2008;1:221–7.
[5] Koren I, Kaufman YJ, Remer LA, Martins JV. Measurement of the effect of Amazon smoke on inhibition of cloud formation. Science 2004;303:1342–5.
[6] Scholes M, Andreae MO. Biogenic and pyrogenic emissions from Africa and their impact on the global atmosphere. Ambio 2000;29: 23–9.
[7] Streets DG, Gupta S, Waldhoff ST, Wang MQ, Bond TC, Bo Y. Black carbon emissions in China. Atmos Environ 2001;35:4281–96.
[8] Giorgi F, Bi X, Qian Y. Direct radiative forcing and regional climatic effects of anthropogenic aerosols over East Asia: a regional coupled climate-chemistry/aerosol model study. J Geophys Res 2002;107: 4439, doi:10.1029/2001JD001066.
[9] Wu J, Jiang W, Fu C, Su B, Liu H, Tang J. Simulation of the radiative effect of black carbon aerosols and the regional climate response over China. Adv Atmos Sci 2004;21:637–49.
[10] Martins J, Artaxo P, Liousse C, Reid J, Hobbs P, Kaufman Y. Effects of black carbon content, particle size, and mixing on light absorption by aerosols from biomass burning in Brazil. J Geophys Res 1998; 103:32041–50.
[11] Jacobson MZ. A physically-based treatment of elemental carbon optics: implications for global direct forcing of aerosols. Geophys Res Lett 2000;27:217–20.
[12] Kahnert M. Numerically exact computations of the optical properties of light absorbing carbon aggregates for wavelength of 200 nm–12.2 μm. Atmos Chem Phys 2010;10:8319–29.
[13] Witten TA, Sander LM. Diffusion-limited aggregation, a kinetic critical phenomenon. Phy Rev Lett 1981;47:1400–3.
[14] Friedlander SK. Smoke, Dust, and Haze, Fundamentals of Aerosol Dynamics. Second edition. New York: Oxford Univ. Press; 2000.
[15] Meakin P. Formation of fractal clusters and networks by irreversible diffusion-limited aggregation. Phy Rev Lett 1983;51:1119–22.
[16] Iskander MF, Chen HY, Penner JE. Optical scattering and absorption by branched chains of aerosols. Appl Opt 1989;28:3083–91.
[17] Mackowski DW. Calculation of total cross sections of multiple-sphere clusters. J Opt Soc Am A 1994;11:2851–61.
[18] Chylek P, Lesins GB, Videen G, Wong JGD, Pinnick RG, Ngo D, et al. Black carbon and absorption of solar radiation by clouds. J Geophys Res 1996;101:23365–71.
[19] Mackowski DW, Mishchenko MI. Calculation of the T matrix and the scattering matrix for ensembles of spheres. J Opt Soc Am A 1996;13:2266–78.
[20] Xu Y. Gustafson BS. A generalized multiparticle Mie-solution: further experimental verification. J Quant Spectrosc Radiat Transfer 2001;70:395–419.
[21] Gustafson BS, Kolokolova L. A systematic study of light scattering by aggregate particles using the microwave analog technique: angular and wavelength dependence of intensity and polarization. J Geophys Res 1999;104:31711–20.
[22] Fuller KA, Malm WC, Kreidenweis SM. Effects of mixing on extinction by carbonaceous particles. J Geophys Res 1999;104:15941–54.
[23] Petrova EV, Jockers K, Kiselev NN. Light scattering by aggregates with sizes comparable to the wavelength: an application to cometary dust. Icarus 2000;148:526–36.
[24] Liu L, Mishchenko MI. Effects of aggregation on scattering and radiative properties of soot aerosols. J Geophys Res 2005;110: D11211, doi:10.1029/2004JD005649.
[25] Liu L, Mishchenko MI. Scattering and radiative properties of complex soot and soot-containing aggregate particles. J Quant Spectrosc Radiat Transfer 2007;106:262–73.
[26] Liu L, Mishchenko MI, Arnott WP. A study of radiative properties of fractal soot aggregates using the superposition T-matrix method. J Quant Spectrosc Radiat Transfer 2008;109:2656–63.
[27] Liou KN, Takano Y, Yang P. On geometric optics and surface waves for light scattering by spheres. J Quant Spectrosc Radiat Transfer 2010;111:1980–9.
[28] Yang P, Liou KN. Light scattering by hexagonal ice crystals: solutions by a ray-by-ray integration algorithm. J Opt Soc Am A 1997;14:2278–89.
[29] Nussenzveig HM, Wiscombe WJ. Efficiency factor in Mie scattering. Phy Rev Lett 1980;45:1490–4.
[30] Toon OB, Ackerman TP. Algorithms for the calculation of scattering by stratified spheres. Appl Opt 1981;20:3657–60.
[31] Takano Y, Liou KN. Solar radiative transfer in cirrus clouds. Part I. Single-scattering and optical properties of hexagonal ice crystals. J Atmos Sci 1989;46:3–19.
[32] Takano Y, Liou KN. Radiative transfer in cirrus clouds. III. Light scattering by irregular ice crystals. J Atmos Sci 1995;52:818–37.
[33] Takano Y, Liou KN. Phase matrix for light scattering by concentrically stratified spheres: comparison of geometric optics and the "exact" theory. Appl Opt 2010;49:3990–6.
[34] Cox C, Munk W. Measurement of the roughness of the sea surface from photographs of the sun's glitter. J Opt Am Soc 1954;44: 838–50.
[35] Strawa AW, Drdla K, Ferry GV, Verma S, Pueschel RF, Yasuda M, et al. Carbonaceous aerosol (Soot) measured in the lower stratosphere during POLARIS and its role in stratospheric photochemistry. J Geophys Res 1999;104:26753–66.
[36] Stratmann F, Bilde M, Dusek U, Frank GP, Hennig T, Henning S, et al. Examination of laboratory-generated coated soot particles: an overview of the LACIS Experiment in November (LExNo) campaign. J Geophys Res 2010;115:D11203, doi:10.1029/2009JD012628.
[37] Mandelbrot BB. The Fractal Geometry of Nature. New York: Freeman; 1983.
[38] Born M, Wolf E. Principles of Optics. Oxford: Pergamon Press; 1975.
[39] Liou KN. An Introduction to Atmospheric Radiation. 2nd edition. San Diego: Academic Press; 2002.
[40] Takano Y, Asano S. Fraunhofer diffraction by ice crystals suspended in the atmosphere. J Meteorol Soc Jpn 1983;61:289–300.
[41] van de Hulst HC. Light Scattering by Small Particles. New York: Wiley; 1957.
[42] Yee SK. Numerical solution of initial boundary value problems involving Maxwell's equations in isotropic media. IEEE Trans Antennas Propag 1966;14:302–7.
[43] Yang P, Liou KN. Finite-time domain method for light scattering by small ice crystals in three-dimensional space. J Opt Soc Am A 1996;13:2072–85.
[44] Yang P, Wei H, Huang H-L, Baum BA, Hu YX, Kattawar GW, et al. Scattering and absorption property database for nonspherical ice particles in the near- through far-infrared spectral region. Appl Opt 2005;44:5512–23.
[45] Yang P, Liou KN. A geometric-optics/integral-equation method for light scattering by nonspherical ice crystals. Appl Opt 1966;35: 6568–84.
[46] Purcell EM, Pennypacker CR. Scattering and absorption of light by nonspherical dielectric grains. Astrophys J 1973;186:705–14.
[47] Draine BT, Flatau PJ. Discrete-dipole approximation for scattering calculations. J Opt Soc Am A 1994;11:1491–9.
[48] Draine B.T., Flatau, P.J. User Guide to the Discrete Dipole Approximation Code DDSCAT 7.1, 2010.〈http://arxiv.org/abs/1002.1505v1〉.
[49] Bond TC, Bergstrom RW. Light absorption by carbonaceous particles: an investigative review. Aerosol Sci Technol 2006;40:27–67.
[50] Sorensen CM. Light scattering by fractal aggregates: a review. Aerosol Sci Technol 2001;35:648–87.
[51] Sheridan PJ, Arnott WP, Ogren JA, Andrews E, Atkinson DB, Covert DS, et al. The Reno aerosol optics study: an evaluation of aerosol absorption measurement methods. Aerosol Sci Technol 2005;39: 1–16.
[52] Wiscombe WJ, Warren SG. A model for the spectral albedo of snow. I. pure snow. J Atmos Sci 1980;37:2712–33.
[53] Warren SG, Wiscombe WJ. A model for the spectral albedo of snow. II: snow containing atmospheric aerosols. J Atmos Sci 1980;37: 2734–45.